Use of FEA derived impedances to design active structures

Andrew G. Littlefield, James A. Fairweather, Kevin C. Craig

Department of Mechanical Engineering, Aeronautical Engineering, & Mechanics

Rensselaer Polytechnic Institute, Troy, NY 12180

Correspondence should be addressed to Kevin Craig, Phone: 518-276-6626, FAX: 518-276-4860, craigk@rpi.edu

Keywords: impedance method, piezoelectric materials, smart structures, finite element method, modeling

ABSTRACT

Previously, the impedance method has been applied to simple structures by determining the modal response using closed-form methods. The present work uses finite element analysis (FEA) to generate the host structure's mechanical impedances from eigenvectors. Two-dimensional structures are studied, though the method should be extendable to any structure that can be modeled by FEA. The equations to recover the impedances and structure's response from an FEA normal mode analysis are developed. The method is then experimentally verified for plates with different boundary conditions, material types, and actuator orientations. The method is found to accurately predict the plate's response.

INTRODUCTION

With the increased use of induced strain actuators, such as piezoelectric ceramics (PZT), comes the demand for more accurate and usable modeling methods. For a method to be effective, it must be easy to use, capture the dynamics of the physical system, and yield accurate predictions of the system's dynamic response. Until recently, all of the methods have failed to meet some or all three of these requirements. The available methods for modeling PZT actuators include static equivalent force (SEF) method (Crawley and de Luis, 1987; Liang, Sun, and Rogers, 1993b; Lalande, 1995; Zhou, Liang, and Rogers, 1996), finite element methods (FEM) (Alik and Hughes, 1970; McDearmon, 1984; Crawley and Anderson, 1989; Hagood, Chung, and von Flotow, 1990), methods derived from first principles (Hagood Chung, and von Flotow, 1990;

Akella, 1994; Pan, Hansen, and Snyder, 1991) and impedance methods (Liang, 1993; Liang, Sun, and Rogers, 1993b; Zhou, Liang, and Rogers, 1993; Zhou, Liang, and Rogers, 1994)

SEF methods are widely used due to their easy formulation and retention of physical insight into the system. When used as "quasi-static" models, in which the pure mechanical strain in the beam at the actuation locations is ignored (modal or external loading strains), the models are very simple. The moment that the actuator can exert on the structure for a given field level is applied as a sinusoidal driving load and the structural response is calculated. In this form, SEF models have been shown to significantly miscalculate the system resonant frequencies, and the actuator force, stress, and strain (Liang, Sun, and Rogers, 1993b; Zhou, Liang, and Rogers, 1996). No attempt is made to include the stiffness, mass or frequency response of the actuator in the model.

There are numerous ways to include PZT actuators in finite element analysis (FEA) models. Some FEM codes, such as ABAQUS, Ansys, and ATILA, have element formulations that include electrical degree of freedoms and couple the electrical field to the strain field in the actuator. In commercial codes that do not provide piezoelectric elements, the PZT's properties have been included into the FEA program directly through custom elements (Alik and Hughes, 1970; McDearmon, 1984; Crawley and Anderson, 1989; Hagood, Chung, and von Flotow, 1990). Another approach is to incorporate the excitation as a local thermal expansion (Liang and Rogers, 1989; Hagood, Chung, and von Flotow, 1990; Ha, Keilers, and Chang, 1992; Mollenhauer and Griffin 1994). The thermal expansion approach is only useful for a static case unless the FEA package has harmonic thermal expansion analysis. While FEM is accurate, it can be very computationally expensive when testing multiple actuator locations and there is often a loss of physical insight into the system.

The use of first principles can allow for both the mechanical and electrical aspects of the actuator to be taken into account. Which aspects and to what degree, depend upon the principle applied. Models using first principle analysis include those based on the Rayleigh-Ritz energy method (Hagood, Chung, and von Flotow, 1990; Akella, 1994) and Bernoulli-Euler beam theory (Crawley and de Luis, 1987; Pan, Hansen, and Snyder, 1991). They have been implemented using finite element, finite difference and Galerkin methods for beams, plates, and shells with piezoceramic sensors/actuators (Banks, Smith, and Wang, 1996; del Rosario and Smith, 1997). First principle based models have been shown to yield results equivalent ot impedance method based models (Wang and Slater, 1998). The drawback to the approach is that the modeling approach explicitly includes the actuator in the formulation of the equations of motion. The dynamics of the structure and actuator are

solved simultaneously, so for every change in actuator placement, the problem must be solved again. This factor makes them ill suited for typical design studies, such as optimal placement of actuators.

The impedance method, as developed at Virginia Polytechnic Institute (Liang, 1993), provides a systematic modeling approach that comes close to meeting the three requirements of a generalized, accurate, and easy-to-use active material modeling system. The mechanical impedance of the host structure is used to determine the load at the actuator boundary. The mechanical impedances are then used to solve for the behavior the actuator to and to determine the dynamic response of the system. Impedance models have been shown to have very good agreement with experimental results (Rossi, Liang, and Rogers, 1993; Sermoneta et al. 1995; Zhou, Liang, and Rogers, 1996).

An advantage of this method is that since the structure's impedance is found independent of the actuator, it is easy to try out different actuator locations. A drawback to this method is the determination of the structure's mechanical impedances. To date, the literature has demonstrated the modeling approach by solving the host structural vibration problem in closed form, and then coupling the analytical impedances to the analytical impedance boundary model of the actuator. Such an approach limits the method’s applicability to simple geometries for which such solutions of the mechanical impedance can be found.

The approach presented in this paper uses FEA to generate the structure's impedances. The impedance method is thus extended to any structure that can be accurately modeled by FEA. Fairweather (1998) developed and experimentally verified the incorporation of FEA impedances in the impedance solution for PZT driven beams. For plates he laid out the equations and compared the predictions to previously published experimental data. In this work a more detailed experimental investigation is provided to verify the predictive capability of the method for two-dimensional structures with arbitrary boundary conditions.

First, the equations to recover the impedances and structure's response from a FEA normal mode analysis are developed. The method is experimentally verified for plates with different boundary conditions, material types, and actuator orientations. Comparisons are made between calculations of the impedances using the eigenvectors at the center points of the patch sides and impedances calculated using a shape function to describe the eigenvectors along the patch sides. Experimental measurements are compared to theoretical predictions.

MODELING OF THE PIEZOELECTRIC CERAMIC PATCH

Zhou, Liang, and Rogers (1996) give a detailed derivation of the solution for the actuator's vibration problem. The moments and forces the PZT patch applies to the structure are expressed in terms of the structure's impedances. The main steps of the prior work will be presented here.

The following assumptions are made for the PZT actuator:

- It undergoes an extensional vibration in two dimensions.
- The electrical field applied to the actuator is spatially uniform over the electrodes of the patch.
- The material is isotropic in the x-y plane.

The equations of motion are found by summing the stresses on a two dimensional differential element. Using the above assumptions and using the constitutive equations to express the stresses, Zhou, Liang, and Rogers (1996) derived the following equations of motion:

$$\frac{Y^E}{1-n_p^2}\frac{\partial^2 u}{\partial x_p^2}+\frac{Y^E}{2(1-n_p)}\frac{\partial^2 v}{\partial x_p \partial y_p}+\frac{Y^E}{2(1+n_p)}\frac{\partial^2 u}{\partial y_p^2}=r_p\frac{\partial^2 u}{\partial t^2} \tag{1}$$

$$\frac{Y^E}{1-n_p^2}\frac{\partial^2 v}{\partial y_p^2}+\frac{Y^E}{2(1-n_p)}\frac{\partial^2 u}{\partial x_p \partial y_p}+\frac{Y^E}{2(1+n_p)}\frac{\partial^2 v}{\partial x_p^2}=r_p\frac{\partial^2 v}{\partial t^2}, \tag{2}$$

where Y^E is the patch's modulus of elasticity, n_p is its Poisson's ratio, and r_p is its density.

These coupled equations describe a classical problem in elasticity, one that was shown by Love (1944) to have a complete analytical solution if the material domain is bounded by a circle.

However in this case we have a rectangular or square patch, complicating the solution. Additionally, the boundary conditions are in terms of the structure's impedances. Zhou, Liang, and Rogers (1996) solved this problem by neglecting the change of rate of shear strain terms. This reduces the equations to:

$$\frac{Y^E}{1-n_p^2}\frac{\partial^2 u}{\partial x_p^2} = r_p \frac{\partial^2 u}{\partial t^2} \tag{3}$$

$$\frac{Y^E}{1-n_p^2}\frac{\partial^2 v}{\partial y_p^2} = r_p \frac{\partial^2 v}{\partial t^2} \tag{4}$$

which can then be solved by separation of variables with an assumed solution of:

$$u(x_p,t) = f(x_p)q(t) = \left(A\sin\left(\Omega x_p\right) + B\cos(\Omega x_p)\right)e^{jwt} \tag{5}$$

$$v(y_p,t) = f(y_p)q(t) = \left(C\sin\left(\Omega y_p\right) + D\cos(\Omega y_p)\right)e^{jwt}, \tag{6}$$

where Ω is the spatial frequency of the oscillations.

The boundary conditions of the piezoceramic patch are:

$$u(0,t) = 0 \quad v(0,t) = 0 \tag{7}$$

which leads to $B = D = 0$. It should be noted that these boundary conditions are not always valid and care should be taken that they are applied appropriately (Wang and Slater, 1998).

A and C can then be found by substituting the assumed solution into the constitutive equations with the stresses expressed in terms of the structure's impedances. This constitutive equation is:

$$\begin{bmatrix} \frac{\partial u}{\partial x_p} \\ \frac{\partial v}{\partial y_p} \end{bmatrix} = -\frac{1}{\tilde{Y}_{11}^E}\begin{bmatrix} 1 & -n_p \\ -n_p & 1 \end{bmatrix}\begin{bmatrix} \frac{1}{A_x} & 0 \\ 0 & \frac{1}{A_y} \end{bmatrix}\begin{bmatrix} Z_{xx} & Z_{xy} \\ Z_{yx} & Z_{yy} \end{bmatrix}\begin{bmatrix} \dot{u} \\ \dot{v} \end{bmatrix} + \begin{bmatrix} d_{31} \\ d_{32} \end{bmatrix}E_3 \tag{8}$$

where E_3 is the applied electric field.

When Equations (5) and (6) are substituted into this and evaluated at $x_p = a_p$ and $y_p = b_p$ one obtains:

$$\begin{bmatrix} A \\ C \end{bmatrix} = \begin{bmatrix} \Omega\cos(\Omega a_p) + \frac{jwZ_{xx}\sin(\Omega a_p)}{Y^E A_x} - \frac{jwn_p Z_{yx}\sin(\Omega a_p)}{Y^E A_y} & \frac{jwZ_{xy}\sin(\Omega b_p)}{Y^E A_x} - \frac{jwn_p Z_{yy}\sin(\Omega b_p)}{Y^E A_y} \\ \frac{jwZ_{yx}\sin(\Omega a_p)}{Y^E A_y} - \frac{jwn_p Z_{xx}\sin(\Omega a_p)}{Y^E A_x} & \Omega\cos(\Omega b_p) + \frac{jwZ_{yy}\sin(\Omega b_p)}{Y^E A_y} - \frac{jwn_p Z_{xy}\sin(\Omega b_p)}{Y^E A_x} \end{bmatrix}^{-1} \begin{bmatrix} d_{31} \\ d_{32} \end{bmatrix} E_3 \tag{9}$$

These expressions are a revision of those presented by Zhou, Liang, and Rogers (1996). The Z_{ij} give the mechanical impedances of the structure. Using these expressions and the assumed displacement solutions, Equations (5) and (6), the force output in terms of the impedance of the mechanical structure is:

$$\begin{bmatrix} F_{a_p} \\ F_{b_p} \end{bmatrix} = -jw \begin{bmatrix} Z_{xx} & Z_{xy} \\ Z_{yx} & Z_{yy} \end{bmatrix} \begin{bmatrix} A\sin(\Omega a_p) & 0 \\ 0 & C\sin(\Omega b_p) \end{bmatrix} e^{jwt}, \tag{10}$$

where coefficients A and C are given by Equation (9). The moment exerted by the patch on the structure is found by using the geometric relationship between force and moment.

$$\begin{bmatrix} M_{a_p} \\ M_{b_p} \end{bmatrix} = -jw\left(t_p + h_p\right) \begin{bmatrix} Z_{xx} & Z_{xy} \\ Z_{yx} & Z_{yy} \end{bmatrix} \begin{bmatrix} A\sin(\Omega a_p) & 0 \\ 0 & C\sin(\Omega b_p) \end{bmatrix} e^{jwt} \tag{11}$$

The force and moment exerted by the PZT patch have been determined in terms of the host structure's mechanical moment impedance; the mechanical moment impedances themselves must be determined.

DETERMINATION OF THE MOMENT IMPEDANCES FROM FEA

Since the impedances are to be determined using MSC/Nastran, the next step is to develop a means to extract the frequency response functions from MSC/Nastran. To do this it is necessary to develop a relationship between the eigenvectors of a node and the forces, moments, velocities and displacements associated with that node.

Consider the following sets of undamped spring mass systems:

$$[M]\ddot{\mathbf{x}} + [K]\mathbf{x} = \mathbf{f(t)}, \tag{12}$$

where $\mathbf{x}$ and $\mathbf{f(t)}$ are (n x 1) vectors describing the physical positions and time varying forcing functions applied to each degree of freedom of the system. Assume that:

- Mass matrix is non-singular.
- Mass and stiffness matrices are symmetric.

Taking the equation to the Laplace domain yields:

$$[M]s^2\mathbf{X(s)} + [K]\mathbf{X(s)} = \mathbf{F(s)} \tag{13}$$

Define a set of eigenvalues, $[\Lambda]$, and mass-normalized eigenvectors, $[\Phi]_n^T$, such that:

$$\mathbf{Q}(s)s^2 - [\Lambda]\mathbf{Q(s)} = [\Phi]_n^T\mathbf{F(s)}\,. \tag{14}$$

The motion of the system in the physical coordinate system can be obtained through the coordinate transformation,

$$\mathbf{X}(s) = [M]^{-\frac{1}{2}}[\Phi]\mathbf{Q}(s) = [\Phi]_n\mathbf{Q}(s)\,, \tag{15}$$

so that:

$$\mathbf{X}(s) = [\Phi]_n\left([I]s^2 - [\Lambda]\right)^{-1}[\Phi]_n^T\mathbf{F(s)} \tag{16}$$

This is the equation relating the displacement vector in physical coordinates to force applied in physical coordinates. For a specific physical coordinate $X_j(s)$ and force $F_k(s)$:

$$\frac{X_j(s)}{F_k(s)} = \sum_{i=1}^{\infty}\frac{[\Phi(j,i)]_{n_X}[\Phi(k,i)]_{n_F}}{s^2 + w_i^2} \tag{17}$$

Differentiating (17) yields the mechanical admittance, the inverse of the mechanical impedance, of the structure:

$$\frac{V_j(s)}{F_k(s)} = \sum_{i=1}^{\infty} \frac{\left[\Phi(j,i)\right]_{n_X} \left[\Phi(k,i)\right]_{n_F} s}{s^2 + w_i^2} \tag{18}$$

This equation for the mechanical admittance makes no requirements on the type of structure, so it can be used for any structure. Since we are interested in plates, we will now show how to get the moment impedances for a plate from Equation (18).

Consider the diagram of the piezoceramic patch attached to a plate structure shown in Figure 1. Inserting the eigenvectors associated with rotation for both the force input and velocity output into Equation (21), one obtains the transfer function between rotational velocity and applied moment. For example, if the eigenvectors associated with rotation about the y-axis at (x_1, y_2) are substituted for both the input and output, one obtains a moment admittance about the y-axis of the structure at the center of the left edge of the patch:

$$\frac{sq_{(x_1,y_2)}(s)}{m_{(x_1,y_2)}(s)} = \sum_{i=1}^{\infty} \frac{\left[\Phi\left(R2_{(x_1,y_2)},i\right)\right]_{n_X} \left[\Phi\left(R2_{(x_1,y_2)},i\right)\right]_{n_F} s}{s^2 + w_i^2}. \tag{19}$$

Using the principal of superposition, one can obtain the admittance transfer function between the differential rotational velocity about the y-axis at points (x_1, y_2) and (x_3, y_2) and counter-posed moments applied at the same points as

$$\frac{s\left[q_{(x_1,y_2)}(s) - q_{(x_3,y_2)}(s)\right]}{\left[m_{(x_1,y_2)}(s) - m_{(x_3,y_2)}(s)\right]} = \sum_{i=1}^{\infty} \frac{\left[\Phi\left(R2_{(x_1,y_2)},i\right) - \Phi\left(R2_{(x_3,y_2)},i\right)\right]_{n_X} \left[\Phi\left(R2_{(x_1,y_2)},i\right) - \Phi\left(R2_{(x_3,y_2)},i\right)\right]_{n_F} s}{s^2 + w_i^2} = H_{xx}, \tag{20}$$

The other H_{ij} are found in a similar fashion and a matrix equation relating differential rotational velocities to the mechanical moment admittances and applied counter-posed moments is written as:

$$\begin{bmatrix} s\Delta q_x(s) \\ s\Delta q_y(s) \end{bmatrix} = \begin{bmatrix} H_{xx} & H_{xy} \\ H_{yx} & H_{yy} \end{bmatrix} \begin{bmatrix} \Delta m_x(s) \\ \Delta m_y(s) \end{bmatrix} \tag{21}$$

Using geometrical relationships Equation (21) can be rewritten to give the applied force as:

$$\begin{bmatrix} \Delta F_{x_p}(s) \\ \Delta F_{y_p}(s) \end{bmatrix} = \frac{2}{(t_p + h_a)^2} \begin{bmatrix} H_{xx} & H_{xy} \\ H_{yx} & H_{yy} \end{bmatrix}^{-1} \begin{bmatrix} s\Delta u(s) \\ s\Delta v(s) \end{bmatrix}, \tag{22}$$

where t_p is the thickness of the plate and h_a is the thickness of the actuator.

The structure's moment impedances are then given as:

$$\begin{bmatrix} Z_{xx} & Z_{xy} \\ Z_{yx} & Z_{yy} \end{bmatrix} = -\frac{2}{(t_p + h_a)^2} \begin{bmatrix} H_{xx} & H_{xy} \\ H_{yx} & H_{yy} \end{bmatrix}^{-1} = \begin{bmatrix} Q_{xx} & Q_{xy} \\ Q_{yx} & Q_{yy} \end{bmatrix}^{-1} \tag{23}$$

where Q_{kl} is defined to be the in plane force admittance.

Utilizing the preceding results the moments exerted by the piezoceramic can be computed from Equation (11) based on the impedances given in Equation (23).

An important point is made with respect to the extensibility of the present modeling approach to problems having non-analytic solutions. As was shown by Banks et al. (1998), the general "combined dynamical system" possessing both continuous and discrete elements does not possess normal modes in the presence of damping except under some very limiting matching conditions. Thus, the present approach, which relies on a normal mode expansion of the host structure dynamics, is prone to modeling error when applied to the general case of the "damped combined dynamical system." The present work does not, therefore, provide a rigorous framework for the analysis of damped non-analytic structures, though its use may still have merit if the analysis can proceed in parallel with experimental validation of the required assumptions. Several options are available if damping is felt to be a significant component of the system dynamic behavior. The simplest of these is to augment the model with modal damping to match the on-resonance response levels. The most obvious drawback to this approach is that the damping/energy dissipation mechanism is non-physical. A second approach is to use a physical damping matrix and apply the modal transformation, recognizing that after transformation the damping matrix will necessarily contain non-diagonal elements. The direct frequency response method in MSC/Nastran can be employed on this system, with a computational benefit gained in that the number of orthogonal modes used to represent the system is likely to be less than the number of physical coordinates in the non-modal solution. A third option is the addition of proportional damping to the finite-element-based series solution based on the use of experimental data, as demonstrated in Griffin et al. (1997). It should be recognized, however, that none of these approaches avoids the fundamental limitation that normal modes will not exist for

this class of system except under the limitations outlined in by Banks et al (1998). Analytic predictions and experimental validation must proceed in lock step when the FEA-based impedance methodology is applied to systems where significant amounts of damping are present.

DETERMINATION OF THE STRUCTURE'S RESPONSE

Now that we have the structure's impedances in terms of its eigenvalues and eigenvectors, we need to develop an equation that will give us the displacement in the z-direction. The vibration response of the plate in terms of eigenvectors is given as:

$$w(x,y,t)=\sum_{m=1}^{\infty}\sum_{n=1}^{\infty}\frac{F_{mn}f_{mn}(x,y)_n}{\left(w_{mn}^2-w^2\right)}Q_t e^{jwt}, \tag{24}$$

where Q_t is the temporal amplitude, which is assumed to be unity, and $f_{mn}(x,y)_n$ are the mass normalized eigenvectors. F_{mn} is the modal force projection and is given as:

$$F_{mn}=-\overline{M}_x\int_{y_1}^{y_3}\left(-\frac{\partial f_{mn}(x,y)_n}{\partial x}\bigg|_{x=x_1}+\frac{\partial f_{mn}(x,y)_n}{\partial x}\bigg|_{x=x_3}\right)dy-\overline{M}_y\int_{x_1}^{x_3}\left(-\frac{\partial f_{mn}(x,y)_n}{\partial y}\bigg|_{y=y_1}+\frac{\partial f_{mn}(x,y)_n}{\partial y}\bigg|_{y=y_3}\right)dx \tag{25}$$

The moments in terms of the structure's impedances are given by Equation (11). To perform this integration it is necessary to have an expression for the spatial derivatives of the eigenvectors in the domains of interest. Under the Kirchoff hypothesis, the spatial derivatives of the are the rotational eigenvectors R1 and R2 (MacNeal, 1994):

$$R1=-\frac{\partial f(x,y)_n}{\partial y} \tag{26}$$

$$R2=\frac{\partial f(x,y)_n}{\partial x} \tag{27}$$

MSC/Nastran reports these at the nodes along the edge of the actuator, so they are fit to a sixth order polynomial so that the integration can be carried out explicitly.

The polynomial can then be integrated to obtain the individual modal force projection in terms of $\overline{M}_x$ and $\overline{M}_y$:

$$w(x,y,t) = \sum_{m=1}^{\infty}\sum_{n=1}^{\infty} \frac{\left(E_{x_n}\overline{M}_x + E_{y_n}\overline{M}_y\right) f_{mn}(x,y)_n}{\left(w_{mn}^2 - w^2\right)} e^{jwt} \tag{28}$$

where E_{x_n} and E_{y_n} are the results of the spatial integration of the rotations about the x-axis and y-axis respectively.

For actuators at an angle to the structure's axis the eigenvectors must be modified. MSC/Nastran reports the eigenvectors in the global coordinate system. The expressions for the force and moments exerted by the patch, determined previously, are expressed in the patch's coordinate system. So the eigenvectors have to be rotated from the global system of the plate to the patch's own coordinate system. Since the Z-axis is the same for both the patch and the plate there is no need to rotate any of the Z quantities back to the global system to find the transverse displacement.

The moment impedances found previously (Zhou, Liang, Rogers, 1996) use eigenvectors from the center of the patch boundaries. This single point may not be a good representation of the entire side of the patch. A better result may be possible by using the entire side of the patch to calculate the moment impedance. As was the case with the modal force projection, we only know the eigenvectors at the nodes, which are discrete points. The same approach is employed as was used with the modal force projection. In fact, the same polynomial used for the modal force projection can be used in computing the impedances. This allows the use of shape functions for calculating the impedances without any extra work.

FEA MODELS

The first step in testing the method is to generate accurate FEA models. Since the method relies on the eigenvectors generated from an FEA model to calculate the impedances, it is important that the model be as accurate as possible. Any errors in the FEA model will cause the final results to be in error.

The models were generated in FEMAP and then run in MSC/NASTRAN. The first model made was for a 6061-T6-aluminum plate bolted at all four corners. CQUAD4 elements were used to model the plate and a normal mode analysis was run to extract the modes. To make sure that this model accurately represents the plate a modal analysis of the actual plate was conducted with an impact hammer. The experimental setup is shown in Figure 2.

The experimentally recovered modes were then compared to the natural frequencies from the FEA model. The difference between the experimental and FEA natural frequencies is shown in Table 1.

This was deemed to be an acceptable fit, so the final models with the different boundary conditions could be made. There were three sets of boundary conditions, one with bolts on four corners, a second with the four bolts plus two additional bolts in the interior, and a third with the holes for the interior bolts but no constraints on the holes. The final models consisted of both CQUAD4 and CTRIA3 elements. The CTRIA3 elements were used when the aspect ratio of the CQUAD4 elements became unacceptable.

The same procedure was followed for the composite plates. The plates were made out of a graphite cloth with a lay up of $[0/90, +45/-45]_s$. The initial results of the modal testing were very unsatisfactory. Differences were found on the order of 50%. It was discovered that the quoted properties for the graphite were for a unidirectional prepreg, whereas the material used was a bi-directional cloth used in a wet lay-up. The only material value that could be experimentally obtained was a bending modulus for the laminate. This result was used in FEMAP and the laminate was entered as 2-D orthotropic material instead of as individual plies. The final results for the modal testing are shown in Table 2.

These results were not as good as those for the aluminum plate but were the best that could be obtained without having better material property data. As in the case of the aluminum plate, there were three sets of boundary conditions, one with bolts on four corners, a second with the four bolts plus two additional bolts in the interior, and a third with the holes for the interior bolts but no constraints on the holes.

The final models again consisted of both CQUAD4 and CTRIA3 elements. The CTRIA3 elements were added automatically by FEMAP whenever the aspect ratio of the CQUAD4 elements was unacceptable. For the coarse models, the mesh sizes varied from 2031 elements to 4158 elements. For the fine models, the mesh sizes varied from 4831 elements to 7785 elements. Model size was limited by available hard disk space on the analysis computer.

EXPERIMENTS AND RESULTS

Four aluminum and two composite plates were made. Two of the aluminum plates had PZT patches aligned with the plate's axis and two had patches at 45 degrees to the plate's axis. For the composite plates there was one aligned and one at 45 degrees. Initially all plates had four holes drilled at the corners and were bolted down at these points. The experimental setup can be seen in Figure 3.

The patches were excited with a sine wave generated by the sine sweep analyzer of a DSPT SigLab. This signal was then passed through an amplifier with a fixed gain of 20. The sine sweep bands and excitation voltages were varied so as to get a good response at each of the first six or so modes. The exact band settings and voltages varied from plate to plate. An eddy current sensor measured the response of the plate and SigLab computed the transfer function. The sensor was located at x = 0.2032 m and y = 0.1524 m as measured from the origin shown in Figure 1. For the composite plate, a button of aluminum was glued to the plate so that the sensor could be used. The button was also added to the FEA model.

Each plate was run twice with just the four corners bolted down. All four bolts were tightened to a torque of 13.56 N·m. This was done to avoid any moments that would be introduced into the plate by uneven tightening of the bolts. After running the tests in the initial configuration, the plates were removed and the interior holes were drilled. The interior bolts were also tightened to a torque of 13.56 N·m. Two runs for each plate were done in this configuration. Two final runs were done on each plate without the interior bolts but with the interior holes.

After collecting all of the data, the experimental transfer functions were then compared to the ones predicted by the impedance method. Several MATLAB m-files were created for this purpose and comparisons were made between evaluating the eigenvectors at the center points versus using shape functions.

Figure 4 shows the experimental versus predicted results for an aluminum plate with a patch aligned with the plate's axis. As can be seen from the plots there is very little difference between using the eigenvectors at the center points of the patch sides and using shape functions to describe the eigenvectors along the patch sides. For the first pole both methods are within 1% of the experimentally found ones. For the second pole they are within 2%. In both cases the difference between measured and predicted is of a similar magnitude as the differences between experimental runs. The differences between the two methods are the magnitudes of the poles. The locations of the poles remain the same in both approaches. Both the coarse and fine meshes produce results that closely track the experimental response. The fine mesh though does do a better job at matching the magnitude of the experimental results and more closely predicts the first zero.

Figure 5 shows the experimental versus predicted results for an aluminum plate with a patch at 45 degrees to the plate's axis. Like the 90-degree case there is practically no difference in predicting the poles between the methods. For the first pole the difference was 2%. For the second pole it was 3%. Though this seems like a larger range than the 90-degree case, the range is due to differences between experimental runs and not predictions. There is one difference between the methods that was

not seen in the 90-degree case. Though it is not readily apparent from the figure, the center point approach predicts extra poles and zeroes that the shape function approach does not. These "extra" poles and zeroes are not found experimentally. By averaging the force application along the edge of the actuator, better prediction of the physical response is achieved.

For the coarse mesh there is a noticeable difference between the predicted magnitudes for using center points vs. shape functions. Both approaches follow the experimental response well up to about 350 Hz. The shape function approach though does a much better job at predicting the correct magnitude of the response. Above 350 Hz though both approaches underestimate the magnitude of the response. In the experimental setup though there was a change in step size around 350 Hz so the problem could arise from this. Using a finer FEA mesh reduces the differences in magnitude between the two approaches.

Figure 6 shows the results for an aluminum plate with a patch aligned with the plate's axis and having interior bolts. There is little difference between the center point and shape function approaches. For the first two poles both methods are less than 1% from the measured pole locations. The shape function approach predicts slightly larger magnitudes and earlier poles and zeroes for the higher frequency modes. Both approaches under predict the pole at 300 Hz by about 5 Hz. However, the shape function approach correctly predicts the next pole, whereas the center point approach misses it by several Hz.

As for the coarse vs. fine FEA mesh issue, in this case there isn't much gained by using a finer mesh. The fine mesh does not do a better job at predicting the occurrence of poles and zeroes but it does do a better job at predicting the magnitudes of them. Other than the magnitude differences at the poles and zeroes the two approaches pretty much mirror each other.

Figure 7 shows the results for an aluminum plate with a patch at 45 degrees to the plate's axis with interior holes. As would be expected this result is very similar to that seen in Figure 4. Both approaches do a good job of following the trend of the experimental response. Both approaches and meshes were off by 3 % for the first pole and less than 1% for the second pole. The use of shape functions does give a better prediction of the magnitude though in most cases the difference between the two approaches is negligible. The use of the finer FEA mesh does once again further improve the performance of the shape function approach.

As was seen with the other 45-degree case, the center point approach predicts extra pairs of poles and zeroes not seen in the shape function approach. These may arise from the rotation of the eigenvectors. Since the shape function approach fits the eigenvectors to a polynomial after the rotation these effects are most likely averaged out.

The results for a composite plate with its actuator aligned with the plate's axis are shown in Figure 8. Overall the predicted response shows the same trends as the experimental results. The agreement is quite good below 175 Hz. To this point the curves lie almost on top of each other. For the coarse mesh the first pole is off by 6% and the second by 2%, for both approaches. For the fine mesh, both approaches were off by 4.5% for the first pole and by 2% for the second one. This difference is within the variation seen between experimental runs. The fourth pole though is under predicted by about 20% by the shape function approach and completely missed by the center point approach, for both mesh densities. This is most likely due to the errors in the composite's material properties. As mentioned previously and shown in Table 2 the error in the material properties caused errors in the higher natural frequencies of the FEA model. Since this same FEA model underlies the impedance model similar errors are to be expected.

As was seen with the aluminum plates when there is a difference between the center point and shape function approaches, it is the shape function approach that shows the better results. Both follow a similar trend but the shape function predictions are closer to the experimental magnitude. The use of a finer FEA mesh further helps the shape function approach to match the experimental magnitude.

SUMMARY

For a modeling method to be useful it must not only give an accurate prediction, but also be easy to use and retain a physical insight into the system. SEF models are easy to use and retain a physical insight into the system but are not very accurate. FEA models are accurate, but require training in specific programs or the ability to write your own custom elements. Also, physical insight can become obscured. First principle approaches produce accurate models and retain physical insight, but for anything more complex than a simple beam or simply supported plate these models become very complex, which makes them ill suited for typical design studies.

Impedance methods are accurate and retain insight, but to date their application has been limited to systems for which closed form expressions of impedance are available. Fairweather (1998) developed a method whereby the impedances could be found from the results of a normal mode FEA. In that work the methodology was applied to a previously analyzed cantilever beam to demonstrate the equivalence of the FEA based approach. For plates he presented the equations and compared the results to the SEF method. Experimental validation was required for problems involving more general geometric constraints and more complex material properties.

In the present work the necessary equations are developed to accommodate different boundary conditions, material symmetries, methods of computing the applied moment, and off axis actuator placement. It is shown that modifications are needed to allow for off-axis actuators. The prior use (Fairweather, 1998) of shape functions to describe edge rotations instead of center point based calculations for the impedances is more thoroughly investigated. Actuator free FEA models of arbitrarily bounded composite plate vibrations are validated. Finally, experimental results comparing FEA-based impedance models to experimental measurements of several piezo driven plate systems are presented.

The results show good agreement between the predicted and measured response of the plate. In most cases there is little or no difference between the shape functions and center point approaches. When there is though (off-axis actuator placement) the shape function calculations yield more accurate results. Shape functions predict more accurate off resonance magnitudes than center point calculations, and seem less prone to generating numerically spurious pole-zero pairs. Since shape function based calculations require little extra work, it is advisable to use them whenever possible.

The effect of mesh density was explored. It was shown that while the method worked reasonably well with a coarse mesh, a finer mesh generated a better match of the magnitude of the response. As always, mesh refinement becomes a trade off between accuracy and computational cost.

Taken altogether these results show that by obtaining the impedances from FEA, the impedance method can be applied to large range of structures. The equations presented are directly applicable for any section of a structure that can be modeled using plate elements.

REFERENCES

Akella, P., Chen, X., Cheng, W., Hughes, D. and Wen, J. 1994, "Modeling and Control of Smart Structures with Bonded Piezoelectric Sensors and Actuators", *Smart Materials and Structures*, 3:344-353.

Allik, H., and Hughes, T. J. R. 1970, "Finite Element Method for Piezoelectric Vibration", *International Journal for Numerical Methods in Engineering*, 2:151 - 157.

Banks, H. T., Luo, Z. H., Bergman, L. A., and Inman, D. J., 1998,"On the existence of normal modes of damped discrete-continuous systems," ASME J. Applied Mechanics, 65, pp 980-989.

Banks, H. T., Smith, R. C., and Wang, Y. 1996, *Smart Material Structures: Modeling, Estimation, and Control*, Masson/John Wiley, Paris/Chichester.

del Rosario, R. C. H., and Smith, R. C. 1997, "Spline Approximation of Thin Shell Dynamics," *International Journal for Numerical Methods in Engineering*, 40, pp. 2807-2840.

Crawley, E. F., and Anderson, E. H. 1989. “Detailed Models of Piezoceramic Actuation of Beams,” *AIAA paper 89-1388-CP*.

Crawley, E. F. and de Luis, J. 1987, "Use of Piezoelectric Actuators as Elements of Intelligent Structures”, *AIAA Journal*, 25(10): 1373 - 1385.

Fairweather, James. 1998, "Designing with Active Materials: an Impedance Based Approach," Ph.D. thesis, Rensselaer Polytechnic Institute, Troy, NY.

Griffin, S. and Henderson, B. 1997, “An investigation into inaccuracies in closed-form piezoceramic actuator models for smart structures,” AIAA 97-1309, 38th AIAA/ASME/ASCE/ASH/ASC Structures, Structural Dynamics, and Materials Conference and Exhibit, April 7-10, Kissimmee, FL.

Ha, S. K., Keilers, C. and Chang, F. 1992, ”Finite Element Analysis of Composite Structures Containing Distributed Sensors and Actuators,” *AIAA Journal*, 30(3).

Hagood, N. W., Chung, W. H., and von Flotow, A. 1990, “Modeling of Piezoelectric Actuator Dynamics for Active Structural Control”, *Journal of Intelligent Material Systems and Structures*, 1(Jul): 327 - 354.

Lalande, F. 1995, “Modeling of the Induced Strain Actuation of Shell Structures,” Ph.D. thesis, Virginia Polytechnic Institute, Blacksburg, VA.

Liang, C., and Rogers, C.A. 1989, “Behavior of Shape Memory Alloy Actuators Embedded in Composites”, *Proceedings of the 1989 International Composites Conference*, Beijing, China, 1-4 Aug., pp. 475-482.

Liang, C., Sun, F.P. and Rogers, C.A. 1993a, “Dynamic Output Characteristics of Piezoelectric Actuators”, *SPIE*, 1916:341-352.

Liang, C., Sun, F.P. and Rogers, C.A. 1993b, “An Impedance Method for Dynamic Analysis of Active Material Systems”, *Collection of Technical Papers- AIAA/ASME Structures, Structural Dynamics, and Materials Conference from the 34th AIAA/ASME/ASCE/AHS/ASC Structures, Structural Dynamics, and Materials Conference*, pp. 3587-3599.

Love, A.E.H. 1944, *Treatise on the Mathematical Theory of Elasticity, Dover Publications*, 4th Edition, New York.

McDearmon, G. F. 1984, “The Addition of Piezoelectric Properties to Structural Finite Element Programs by Matrix Manipulations”, *Journal of the Acoustic Society of America*, 76(3): 666 - 669.

MacNeal, R.H. 1994. *Finite Elements: Their Design and Performance*, Marcel Dekker, Inc., New York.

Mollenhauer, D.H. and Hayden-Griffin, O. 1994, “Induced Strain Actuation of Surface Bonded Piezoceramic Patches: A Numerical and Experimental Study”, *Journal of Intelligent Material Systems and Structures*, 5(May): 355-362.

Pan J., Hansen C.H. and Snyder S.D. 1991, "A Study of the Response of a Simply Supported Beam to Excitation by a Piezoelectric Actuator”, *Recent Advances in Active Control of Sound and Vibration*, edited by Fuller C.R. and Rogers C.A., Virginia Polytechnic Institute, pp. 39-49.

Rossi, A., Liang, C. and Rogers, C.A. 1993, “Impedance Modeling of Piezoelectric Actuator-Driven Systems: An Application to Cylindrical Ring Structures”, *Proceedings, AIAA/ASME/ASCE/AHS/ASC 34th Structures, Structural Dynamics and Materials Conference*, La Jolla, CA, AIAA Publishing, Washington, DC, pp. 3618-3624.

Sermoneta, A., Liang, C., Sun, F. and Rogers, C.A. 1995, “Dynamic Analysis of Active Structures Under Multiple Actuator Excitations using an Impedance Approach”, *SPIE*, 2443:448-457.

Wang, Y. and Slater, J. C., 1998, “A Comparison of Conventional and Impedance Methods for Modeling Piezoelectric Materials Actuation in Smart Structures,” *Journal of Vibration and Acoustics*, 120(July): 685-688.

Zhou S., Liang C. and Rogers C.A. 1993, "Impedance Modeling of Two-Dimensional Piezoelectric Actuators Bonded on a Cylinder", edited by Carman, G.P., and Garcia, E., *Adaptive Structures and Material Systems*, AD- Vol.35, 1993 ASME Winter Annual Meeting, New Orleans, La., Nov. 28 - Dec. 3, pp. 247-255.

Zhou, S., Liang, C. and Rogers, C.A. 1994, "A Dynamic Model of Piezoelectric Actuator-Driven Thin Plates," *Proceeding of the Smart Structures and Materials Conference*, Orlando, SPIE, 2190: pp. 550-562.

Zhou, S., Liang, C. and Rogers, C.A. 1996, "An Impedance-Based System Modeling Approach for Induced Strain Actuator-Driven Structures", *Journal of Vibration and Acoustics*, 118(July): 323-331.

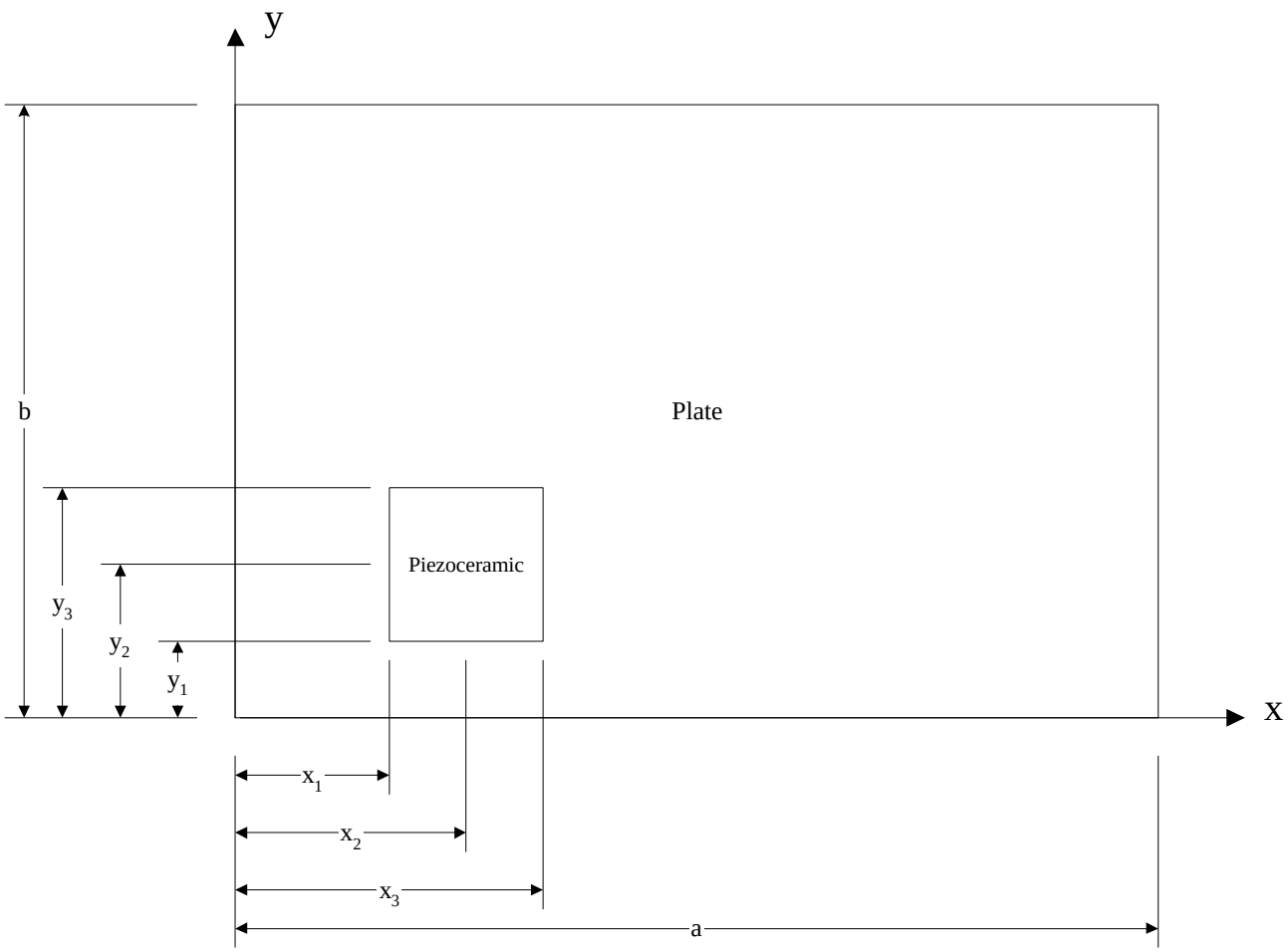

Figure 1: Schematic drawing showing size of plate and location of patch

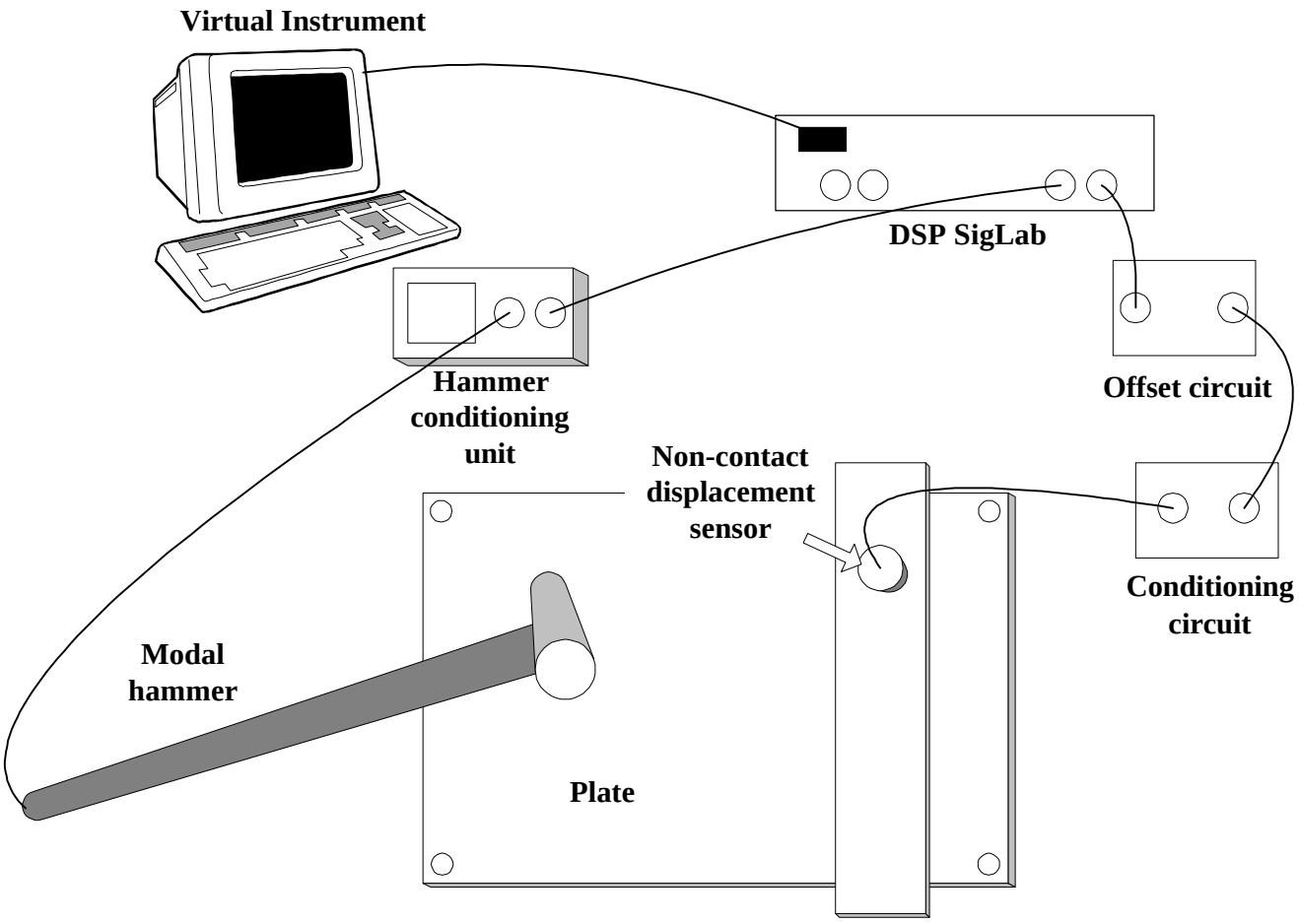

Figure 2: Modal Testing of the Plate

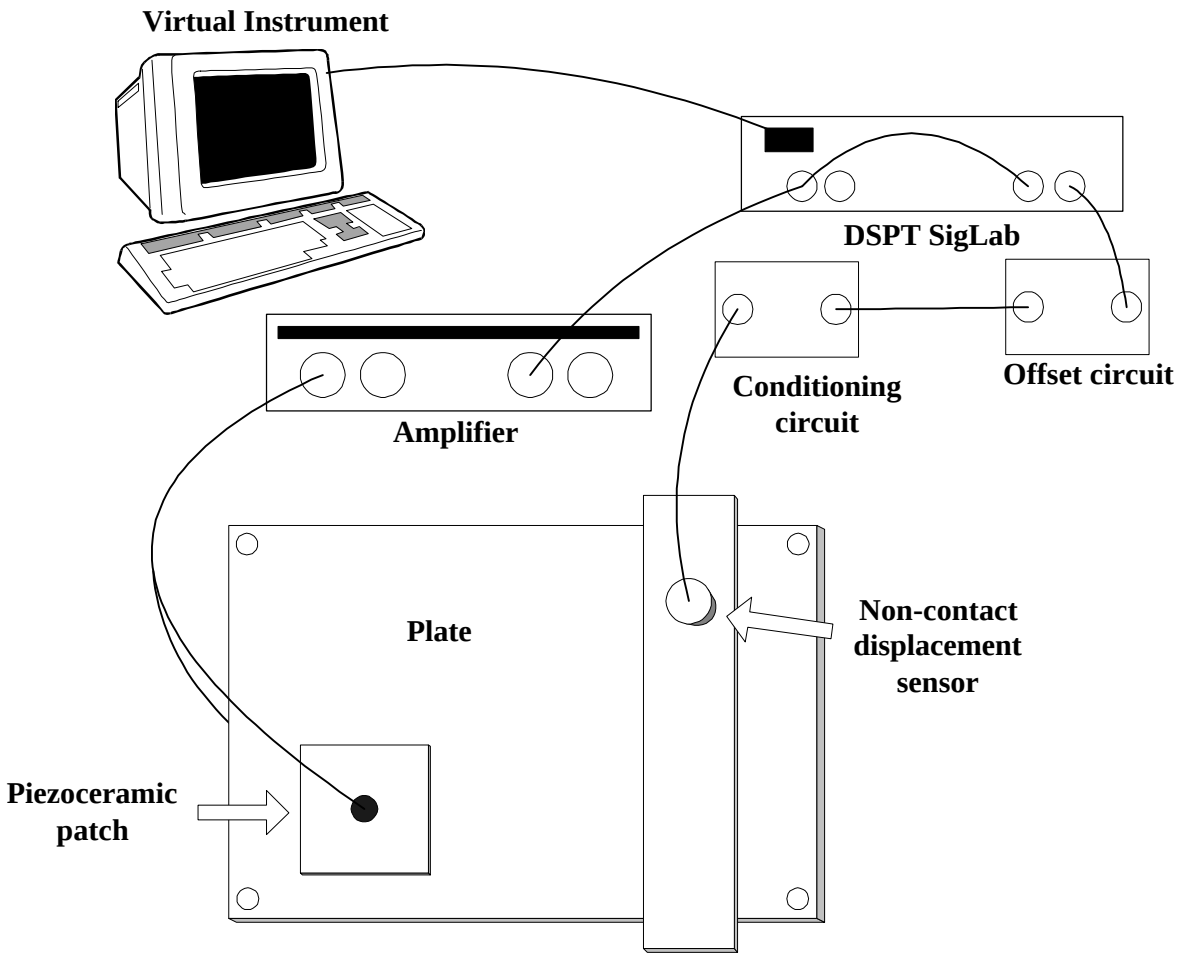

Figure 3: Experimental setup

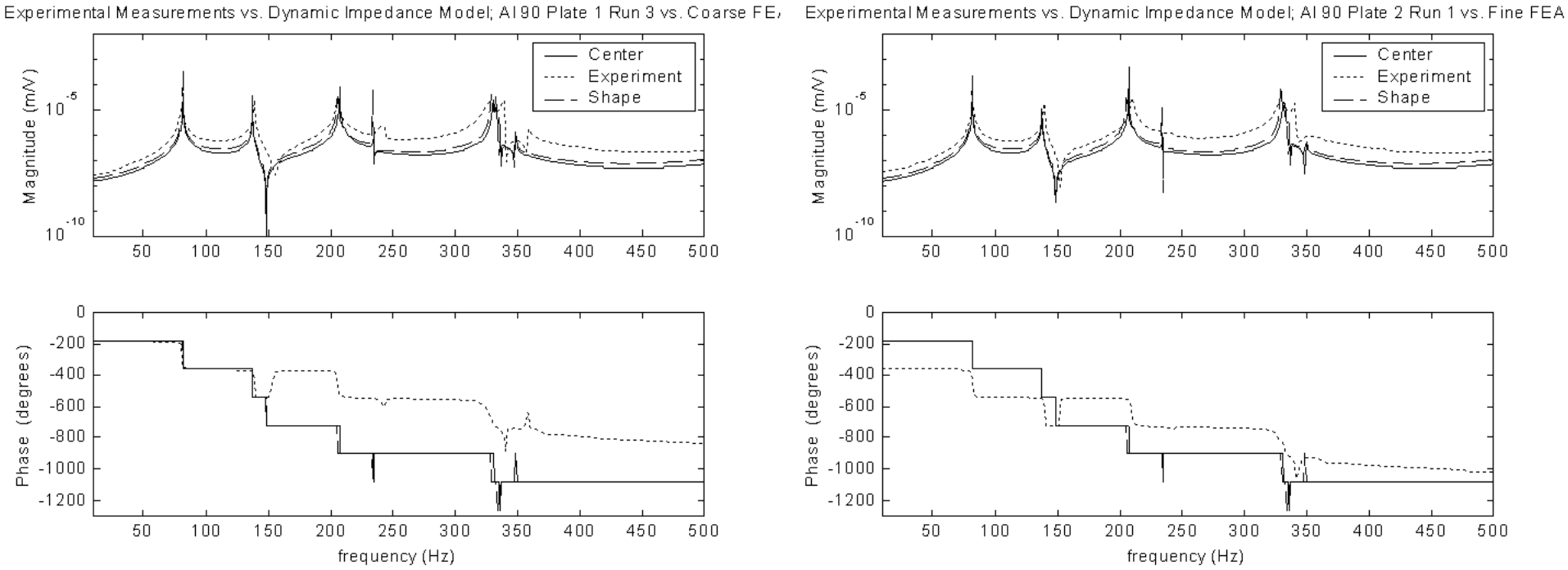

Figure 4: Al plate with 90-degree patch vs. Coarse (left) and Fine (right) FEA

Center Point (solid line), Experiment (dotted), Shape Function (dashed)

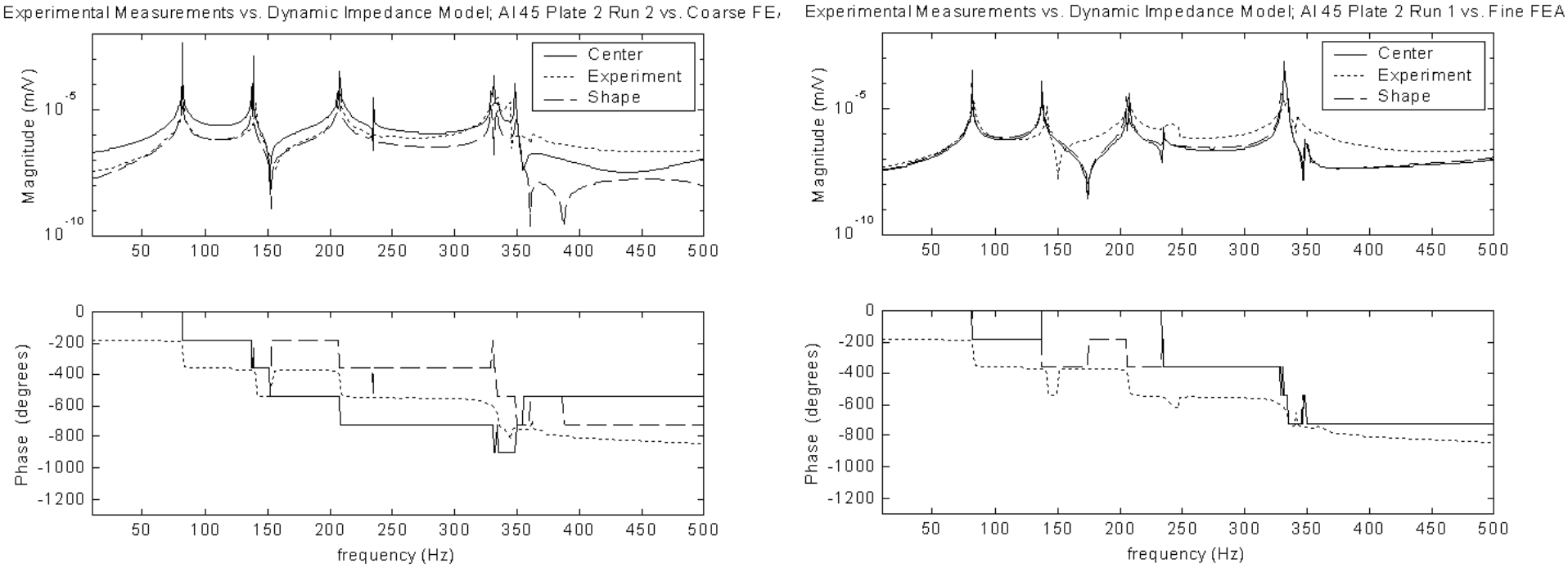

Figure 5: Al plate with 45-degree patch vs. Coarse (left) and Fine (right) FEA

Center Point (solid), Experiment (dotted), Shape Function (dashed)

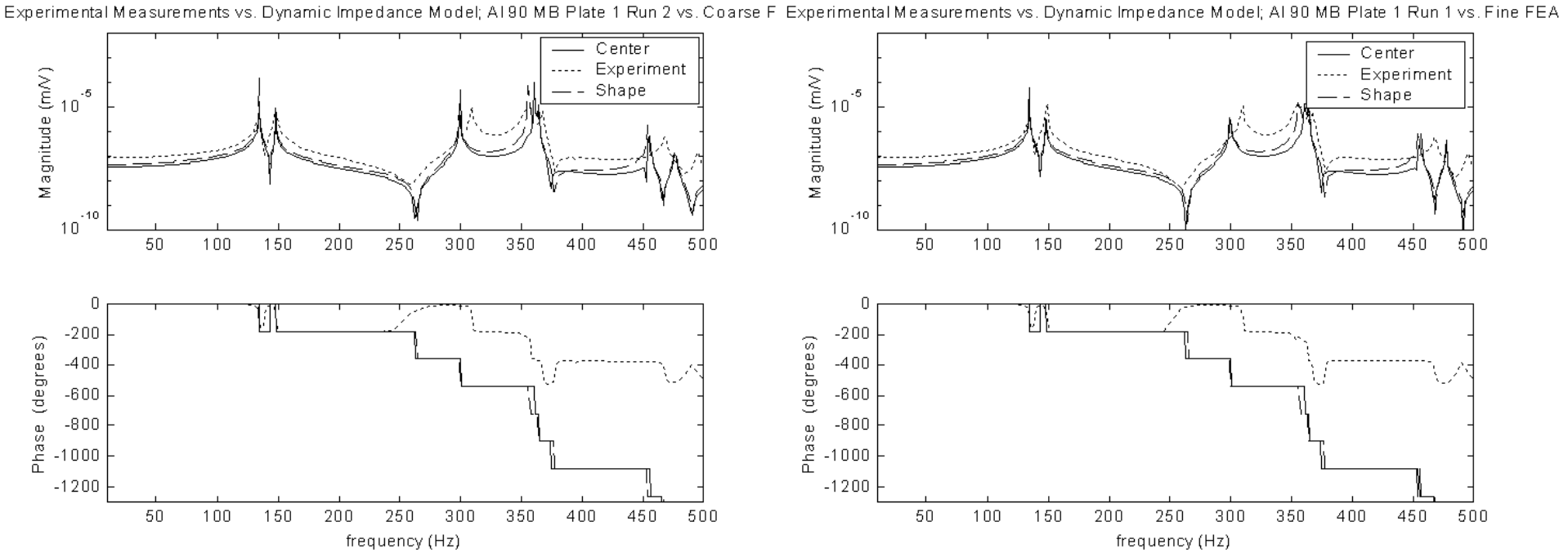

Figure 6: Al plate with 90-degree patch and interior bolts vs. Coarse (left) and Fine (right) FEA

Center Point (solid), Experiment (dotted), Shape Function (dashed)

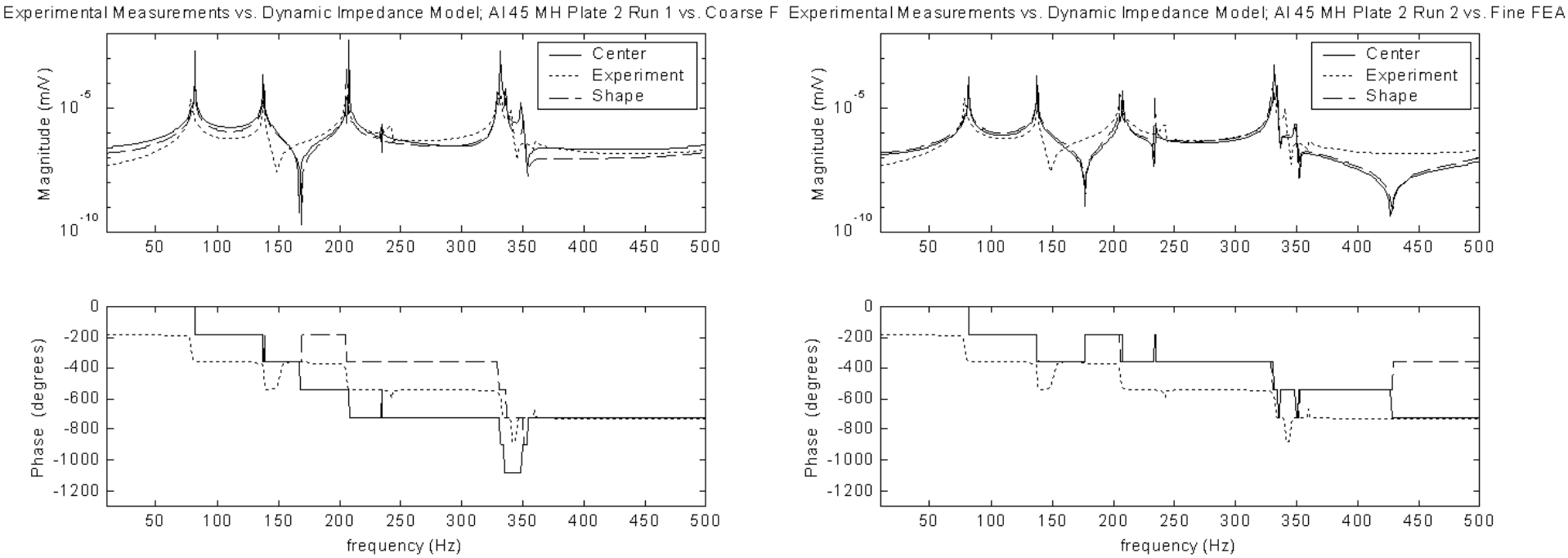

Figure 7: Al plate with 45-degree patch and interior holes vs. Coarse (left) and Fine (right) FEA

Center Point (solid), Experiment (dotted), Shape Function (dashed)

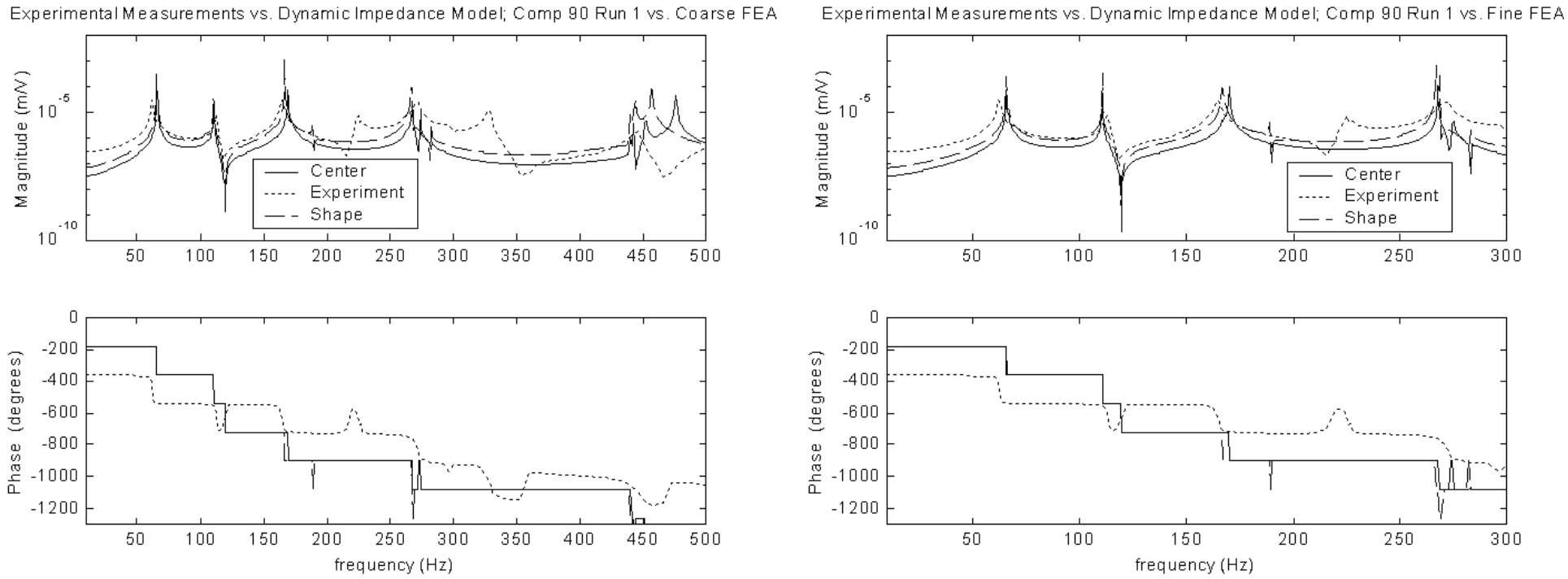

Figure 8: Composite plate with 90-degree patch vs. Coarse (left) and Fine (right) FEA

Center Point (solid), Experiment (dotted), Shape Function (dashed)

Table 1 Difference between predicted and measured natural frequencies

Mode	Measured Frequency (rad/sec)	Predicted Frequency (rad/sec)	Percent Difference
1	81.8750	81.40003	-0.58%
2	137.5000	137.2957	-0.15%
3	210.6250	205.8459	-2.27%
4	240.6250	234.2385	-2.65%
5	334.3750	329.3206	-1.51%
6	338.7500	332.9155	-1.72%
7	356.2500	348.4398	-2.19%

Table 2 Difference between predicted and measured natural frequencies

Mode	Measured Frequency (rad/sec)	Predicted Frequency (rad/sec)	Percent Difference
1	65.5357	65.7899	0.39%
2	111.7708	110.595	-1.06%
3	130.4167	166.8	21.81%
4	175.0000	188.9572	7.39%
5	224.6429	266.1453	15.59%
6	276.9906	267.9463	-3.38%
7	294.1667	282.0647	-4.29%